Journal of Materials Chemistry A

TaO_x electron transport layers for CO_2 reduction Si photocathodes

Journal:	*Journal of Materials Chemistry A*
Manuscript ID	TA-ART-02-2023-001028.R2
Article Type:	Paper
Date Submitted by the Author:	13-May-2023
Complete List of Authors:	Prabhakar, Rajiv Ramanujam; Lawrence Berkeley National Laboratory, Chemical sciences division Lemerle, Raphaël ; École Polytechnique Fédéral de Lausanne Barecka, Magda; Northeastern University College of Engineering, Chemical Engineering; Chem Kim, Minki; Korea Advanced Institute of Science and Technology (KAIST) Seo, Sehun; Lawrence Berkeley National Laboratory, Dayi, Elif Nur; École Polytechnique Fédérale de Lausanne Dei Tos, Irene; Lawrence Berkeley National Laboratory Ager III, Joel; Lawrence Berkeley National Laboratory, Materials Sciences

TaO_x electron transport layers for CO_2 reduction Si photocathodes

Rajiv Ramanujam Prabhakar,[a,b,#] *Raphaël Lemerle,*[a,b,c,#] *Magda Barecka,*[d,e,f] *Minki Kim,*[a,b,g]

Sehun Seo[a,b]*, Elif Nur Dayi,*[a,b,c] *Irene Dei Tos,*[a,b] *and Joel W. Ager,*[a,b,h,i,*]

[a]Liquid Sunlight Alliance, Lawrence Berkeley National Laboratory, Berkeley, California 94720, United States

[b]Chemical Sciences Division, Lawrence Berkeley National Laboratory, Berkeley, California 94720, United States

[c]Materials Science and Engineering, École Polytechnique Fédéral de Lausanne, Lausanne 1015, Switzerland

[d]Department of Chemical Engineering, Northeastern University, 360 Huntington Avenue, 02215 Boston, USA; email: m.barecka@northeastern.edu

[e]Department of Chemistry and Chemical Biology, Northeastern University, 360 Huntington Avenue, 02215 Boston, USA

[f]Cambridge Centre for Advanced Research and Education in Singapore, CARES Ltd., 1 CREATE Way, CREATE Tower #05-05, 138602, Singapore.

[g]Chemical and Biomolecular Engineering, Korea Advanced Institute of Science and Technology (KAIST), Daejeon 34141, Republic of Korea

[h]Department of Materials Science and Engineering, University of California, Berkeley, Berkeley, CA 94720, USA

[i]Materials Sciences Division, Lawrence Berkeley National Laboratory, Berkeley, California 94720, United States

AUTHOR INFORMATION

# These authors contributed equally

Corresponding Author

*jwager@lbl.gov (J. W. Ager)

KEYWORDS: Photoelectrochemistry, CO_2 reduction, charge selective contacts, TaO_x

ABSTRACT

Electron transport layers (ETLs) used as components of photocathodes for light-driven CO_2 reduction (CO_2R) in aqueous media should have good electronic transport, be stable under CO_2R conditions, and, ideally, be catalytically inert for the competing hydrogen evolution reaction (HER). Here, using planar p-Si (100) as the absorbing material, we show that TaO_x satisfies all three of the above criteria. TaO_x films were synthesized by both pulsed laser deposition (PLD) and radio-frequency (RF) sputtering. In both cases, careful control of the oxygen partial pressure during growth was required to produce ETLs with acceptable electron conductivity. p-Si/TaO_x photocathodes were interfaced with ca. 10 nm of a CO_2R catalyst: Cu or Au. Under front illumination with simulated AM 1.5G in CO_2-saturated bicarbonate buffer, we observed, for both metals, faradaic efficiencies for CO_2R products of ~50% and ~30% for PLD TaO_x and RF sputtered TaO_x, respectively, at photocurrent densities up to 8 mA cm^{-2}. p-Si/TiO_2/Cu photocathodes were also evaluated but produced mostly H_2 (>97%) due to reduction of the TiO_2 to Ti metal under CO_2R conditions. In contrast, a dual ETL photocathode (p-Si/TiO_2/TaO_x/Cu) was selective for CO_2R, which suggests a strategy for separately optimizing selective charge collection and the stability of the ETL/water interface. The maximum photovoltage obtained with p-Si/TaO_x/Cu devices was 300 mV which was increased to 430-460 mV by employing ion implantation to make pn^+-SiTaO_x/Cu structures. Photocathodes with RF sputtered TaO_x ETLs are stable for CO_2R for at least 300 min. Techno-economic analysis shows that the reported system, if scaled, could allow for an economically viable production of feedstocks for chemical synthesis under the adoption of specific CO_2 credit schemes, thus becoming a significant component to carbon-neutral manufacturing.

INTRODUCTION

Charge selective contacts (CSC) provide the asymmetric necessary for light to electrical power conversion in photovoltaic (PV) solar cells.[1] For this reason, in silicon PV there is significant research focus and progress on engineering CSCs that provide both efficient charge collection and interface passivation.[2–5] Energy conversion with photoelectrochemical (PEC) devices operates on the same principle: the surfaces of photocathodes must be selective for electrons and the surface of photoanodes must be selective for holes. While some materials, notably metal oxides used as photoanodes for the oxygen evolution reaction (OER), provide charge selectivity via their intrinsic catalytic activity for the desired reaction, engineered surface layers are also widely employed.[6,7]

For PEC electrodes, in addition to charge carrier selectivity, there are two additional constraints for CSCs. Firstly, the CSC must be stable in the electrochemical environment (often either strong base or acid) so that it can serve as a "protection" layer for the photoabsorber if it is a kinetically or thermodynamically unstable material during operation.[8] Further, the CSC either by itself or in combination with a co-catalyst must provide selectivity to the desired reaction, for instance hydrogen evolution reaction (HER), oxygen evolution reaction (OER) or CO_2 reduction (CO_2R). Additionally, for the case of PEC CO_2R, since both HER and CO_2R are thermodynamically possible, the CSC or, more specifically, the electron transport layer (ETL) in combination with a co-catalyst must be selective to CO_2R products rather than HER.

There are numerous experimental reports which utilize a Si/ETL/co-catalyst stack to form photocathodes for HER.[9–11] TiO_2 and either Pt or Ru are typical choices for the ETL and HER catalyst, respectively. To make a photocathode which will instead reduce CO_2, the co-catalyst should be replaced with a metal which is more active for CO_2R than for HER.[12,13] For instance, Au has been reported to drive CO_2R more selectively towards CO,[14] Bi towards formate,[15,16] and Cu towards C-C coupled products like C_2H_4.[13,17] However, there are comparatively fewer reports on the functioning of these catalysts when integrated with CO_2R photocathodes. Hinogami et al.[18] interfaced p-Si with Cu, Ag, and Au without any ETL and found faradaic efficiencies (FEs) of up to ca. 30% for formate and methane for Cu and up to 50% for CO for Ag. Qiu et al.[19] reported a p-InP/TiO_2/Cu photocathode which, intriguingly, produced methanol at ca. 5% FE. Gurudayal et al.[20] reported a Si photocathode with a TiO_2 ETL and Cu-Ag bimetallic catalyst which produced up to 80% selectivity for C_2+ products. However, in this case, the thick catalyst layer was optically opaque so that illumination from the back (dry) side was employed.

It thus remains an unmet challenge to make a selective CO_2R photocathode capable of front (wet) side illumination. Having an optically thin co-catalyst layer would minimize the photoelectrode cost and allowing for the photocathode to be illuminated from the front side (wet side).[21] This would be particularly advantageous when employing low-cost light absorbers with short minority carrier diffusion lengths. In our initial attempts to make such a device we used p-Si/TiO_2 interfaced with Cu and Ag. However, under operation, the TiO_2 was reduced to Ti metal, which then dominates the catalytic activity and produces H_2 (FE > 97%).

We then examined the Si PV literature to find an oxide ETL which would be more stable than TiO_2; TaO_x appeared promising. When interfaced to Si, it has a small conduction band offset (desirable for electron collection) and large valence band offset (desirable for hole blocking) and is reported to passivate surface states.[22–24] Si PV cells incorporating an n-Si/TaO_x heterocontact have been reported to have up to 19% power conversion efficiency.[22] TaO_x has also been used as an ETL for photocathodes. Wang et al[25] reported that a pn^+-Si/Ta_2O_5/Pt photocathode was stable for over 200 hours while generating H_2. Riyajuddin et al[26] reported 10 hours of stability under HER conditions for a Si nanowire/Ta_2O_5/N-doped graphene quantum dot photocathode.

The prior PV and PEC HER work with TaO_x suggests that it may be a good candidate for an ETL for PEC CO_2R devices. Moreover, examination of its Pourbaix diagram under typical CO_2

reduction (CO_2R) conditions (-1 V vs. SHE and pH 7) predicts that it will be stable.[27,28] There is also considerable synthesis flexibility. TaO_x thin films have been prepared by a variety of techniques like pulsed laser deposition (PLD)[29], RF sputtering[30] and atomic layer deposition (ALD)[31] and its electronic conductivity can be tuned (from insulating to semiconducting) by controlling the concentration of oxygen vacancies.[32]

These considerations motivated us to study p-Si/TaO_x photocathodes interfaced with thin (optically transparent) metal CO_2R catalysts (p-Si/TaO_x/Cu). We synthesized TaO_x thin films using pulsed laser deposition (PLD) and reactive radio frequency (RF) sputtering techniques. Stoichiometric Ta_2O_5 films had poor electronic transport which was improved by controlling the oxygen partial pressure during deposition. Under simulated AM 1.5G illumination, the TaO_x ETL-based Si photocathodes (synthesized by both PLD and RF sputtering) had good selectivity to CO_2R products, ~50% and ~30% respectively, which we attribute to the stability and inertness of the TaO_x. Using ion implanted contacts onto silicon photocathodes with TaO_x ETLs higher photovoltages were obtained (p-Si/n^+/TaO_x/Cu ~ 430 mV and p^+/n-Si/n^+/TaO_x/Cu ~ 460 mV) when compared to p-Si/TaO_x junction (~ 300 mV). We found that the photocathodes were quite sensitive to contamination from metal crossover from the anode due to the small catalyst loading needed for optical transparency and that this could be mitigated by using a non-noble metal counter electrode (graphite). We identify stability as a key challenge for this type of solar to chemical energy conversion approach and provide scale-up scenarios informed by a technoeconomic analysis.

RESULTS AND DISCUSSION

TiO_2 as an ETL for CO_2R Si photocathodes with a thin Cu catalyst. In initial work, we investigated the CO_2R product distribution of a p-Si photocathode with an atomic layer deposition (ALD) TiO_2 as an ETL and a thin 10 nm Cu co-catalyst. PEC measurements were performed in 0.1

M $KHCO_3$ electrolyte under 1 sun illumination for Si photocathodes (these conditions were used throughout the study, see Detailed Methods section in the SI). Such a photocathode shows a photocurrent onset at ~ -0.05 V vs RHE and a photocurrent density of ~ 12 mA cm^{-2} at -1 V vs RHE (**Figure 1a).** However, the expected products from CO_2R on Cu are not observed. Instead, the major product is H_2 (FE >97%, **Figure 1b**).

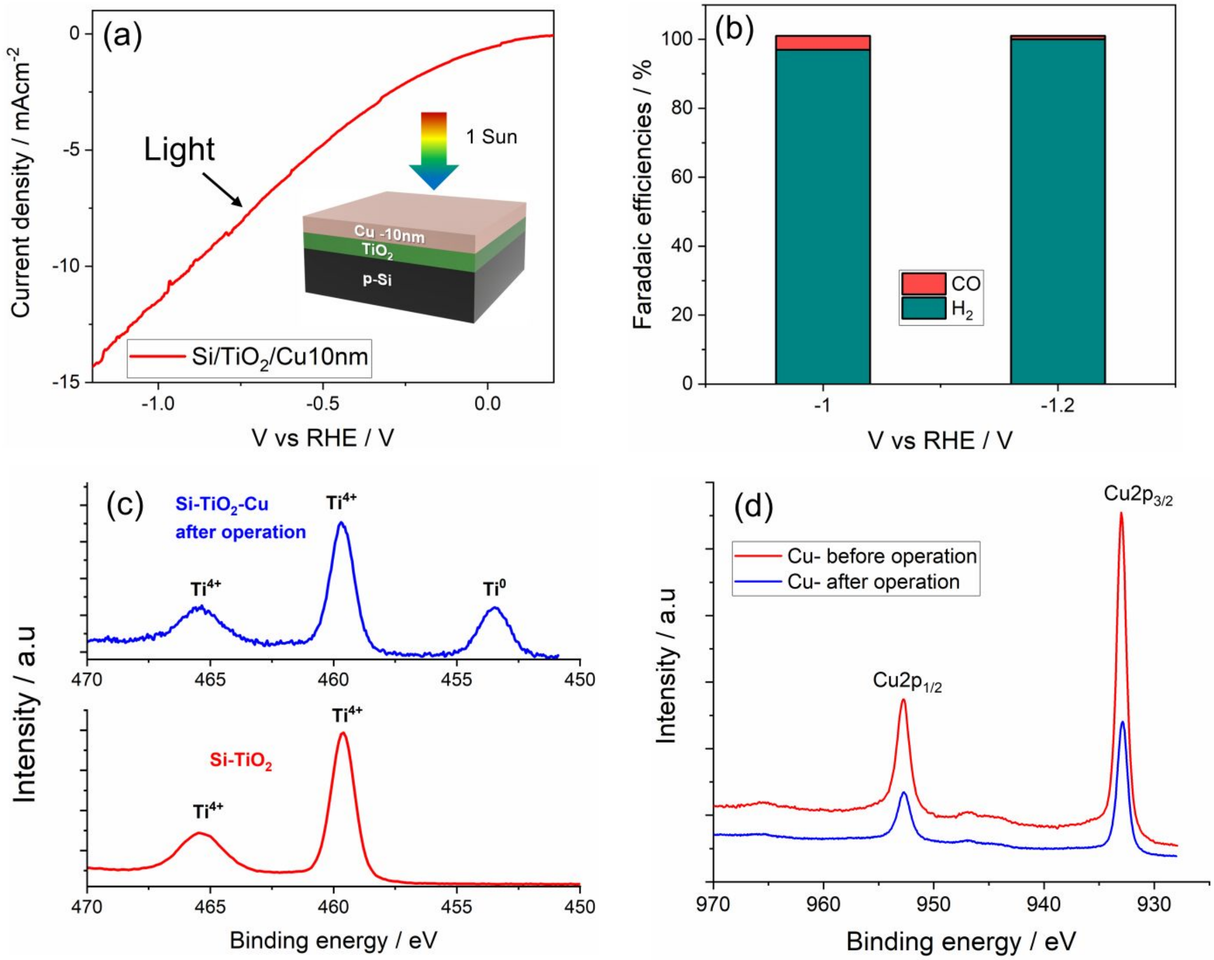

Figure 1. (a) Current density (*J*) vs Voltage (*V*) plots for Si/TiO_2/Cu10 nm under 1 sun illumination in 0.1 M $KHCO_3$ (b) Faradaic efficiencies of CO_2R products for pSi/TiO_2/Cu10 nm (c) Ti 2p core level spectra of Si-TiO_2 (as prepared from ALD) and Si-TiO_2-Cu10nm after CO_2R photo electrolysis for 230 mins under 1 sun illumination in 0.1M $KHCO_3$ at -1.0 V vs RHE (d) Cu 2p

core level spectra of Si-TiO_2-Cu10nm before and after operation under 1 sun illumination in 0.1 M $KHCO_3$ at -1.0 V vs RHE.

We hypothesized that the H_2 formation was due to the activity of Ti metal, which is known to be active for HER.[13] Indeed, we see experimental evidence that when TiO_2 is in contact with the electrolyte (0.1 M $KHCO_3$) under CO_2R conditions, it is reduced to Ti metal as evidenced by the prominent Ti^0 peak in the Ti 2p core level spectra after operation (**Figure 1c**). Before CO_2R operation the TiO_2 was completely covered by the Cu catalyst as evidenced by the absence of Ti XPS peaks (**Figure S2**). However, during CO_2R operation, the TiO_2 layer was gradually exposed to the electrolyte as evidenced by the observation of Ti XPS peaks after operation (**Figure 1c**). Evidently, the HER activity on the Ti outcompetes CO_2R on the Cu, which remain unmodified after operation (**Figure 1d**).

We investigated the effect of increasing the thickness of the Cu layer, understanding that this will eventually limit the photocurrent density in the front illumination geometry which we employed. Upon increasing the Cu thickness to 15 nm (**Figure S3 (a)**), we observed a marginal improvement with CO_2R FEs of ca. 10%. Further increases in the metal thickness would be expected to greatly reduce the photocurrent (**Figure S3 (b)**). We concluded that TiO_2 is not a suitable ETL for CO_2R photocathodes operated under the conditions we have employed and thus explored TaO_x as an alternative.

Pulsed Laser Deposition (PLD) grown TaO_x as an ETL for p-Si CO_2R photocathodes: Next, we synthesized TaO_x films on p-Si by PLD using a stoichiometric Ta_2O_5 target (details in SI). Substoichiometric Ta_2O_5 has been reported to exhibit higher electronic conductivity than more stoichiometric material due to the presence of oxygen vacancies.[33] Therefore, different O_2 flow rates were employed in the PLD chamber as shown schematically in **Figure 2 (a)**. We denote TaO_x grown by PLD on p-Si with 0.1 sccm, 0.3 sccm and 1.6 sccm oxygen flow as TaO_x-0.1, TaO_x-0.3

and TaO_x-1.6. As expected from prior reports on PLD-grown TaO_x without any annealing step,[34] XRD patterns (**Figure S4)** were featureless, indicating that the films are amorphous.

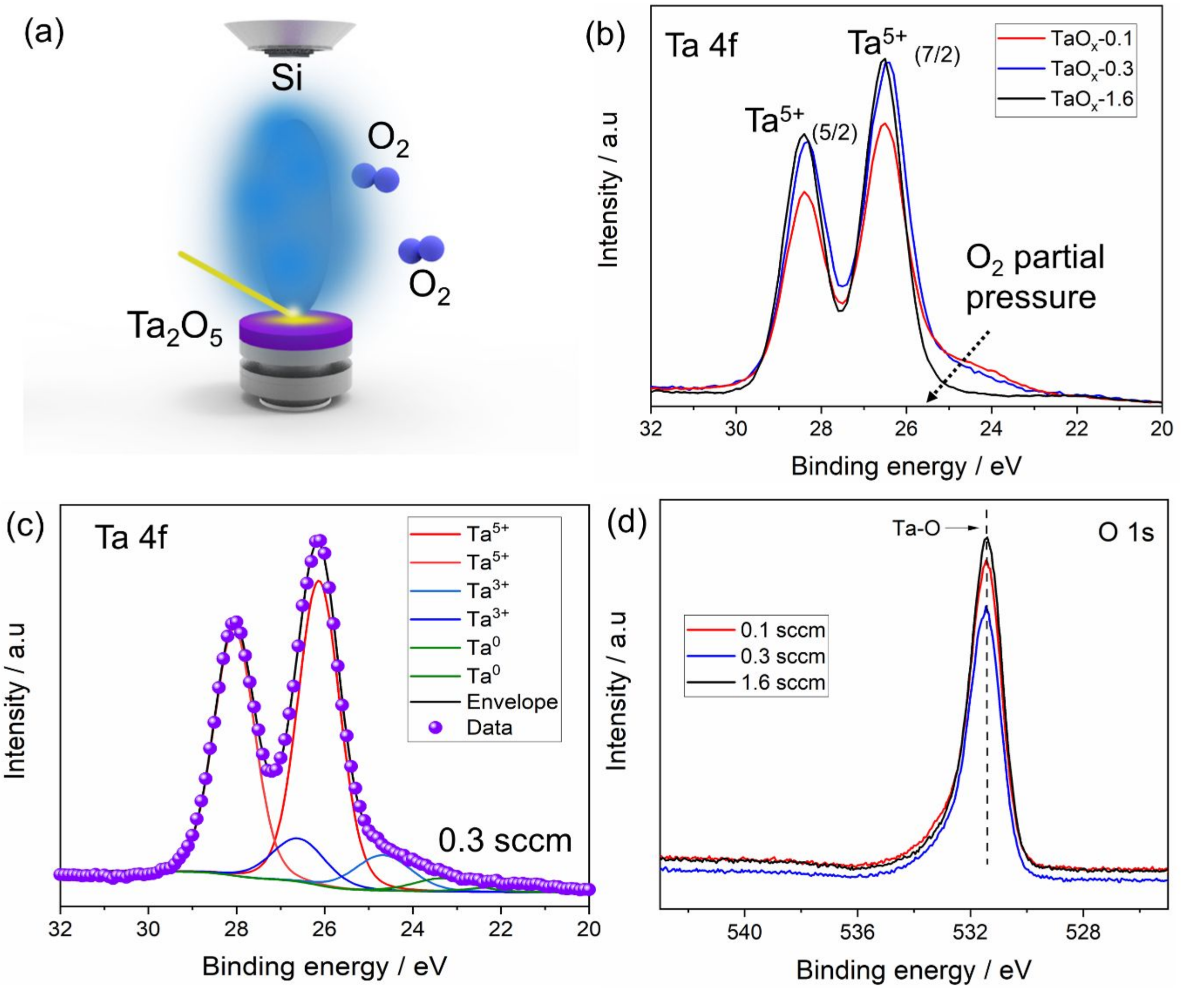

Figure 2. (a) Schematic of PLD deposition of TaO_x (b) XPS core level spectra of Ta 4f for PLD-grown TaO_x grown at different oxygen flow rates (c) XPS core level spectra of Ta 4f for TaO_x-0.3(d) XPS core level spectra of O1s for PLD-grown TaO_x at different oxygen flow rates.

Chemical composition was evaluated with X-ray photoelectron spectroscopy (XPS). We assign the doublet peak observed at 28.3/26.4 eV for all films (**Figure 2 (b)**) to Ta 4f 7/2 and Ta 4f 5/2 from the Ta^{5+} oxidation state.[35] A notable feature of the Ta 4f spectra is the presence of a shoulder peak at between 25 eV and 23 eV which decreases with increasing O_2 flow rate in the PLD chamber. We assign this feature to sub-oxides of Ta which are expected to be formed in substoichiometric Ta_2O_5 films.[36]

Higher flow rates of O_2 (1.6 sccm) yielded a more stoichiometric Ta_2O_5 film as evidenced by the absence of suboxides of tantalum oxide. **Figure 2 (c)** shows the deconvolution of the Ta 4f spectra of TaO_x-0.3. Focusing on the shoulder at lower binding energy, the peaks at 26.4 eV and 24.5 eV are attributed to the Ta^{3+} oxidation state.[30,37] The O 1s spectrum was fitted with two gaussian components with peaks at 530.9 eV and 532 eV which would correspond to Ta-O binding and surface contaminations/ peroxide O_2^{2-} (**Figure S5**).[22,35] No obvious difference was observed for the O 1s spectra for the different O_2 flow rates of the TaO_x films (**Figure 2 (d)**) with the peak position of the Ta-O binding remaining the same for all thin films. Our XPS results shows that the stoichiometry of TaO_x could be controlled by varying the O_2 flow rate in the PLD chamber.

Next, we fabricated p-Si photocathodes with the PLD-grown TaO_x as the ETL and Cu co-catalyst. We chose a Cu catalyst thickness of 10 nm due to higher CO_2R product yield and higher photocurrent density (despite having lower transmission of light to the photocathode than a 5 nm thick Cu co-catalyst) (**Figure S6-S8**). Si photocathodes with a TaO_x-0.3 ETL exhibited the highest photocurrent density under CO_2R conditions reaching a maximum photocurrent density of ~ 7 mA cm^{-2} (**Figure 3 (a)**). The photocurrent density of TaO_x-1.6 was lower than the TaO_x-0.3 due to its higher resistivity as result of a higher oxygen partial pressure during the PLD growth.[32,37]. This was verified by performing ultraviolet photoelectron spectroscopy (UPS) measurements to obtain the valence band spectra of TaO_x (**Figure 3 (b)**). It is evident that the defect band in the band gap of TaO_x increases with reduced oxygen partial pressure confirming the increase of oxygen vacancies for PLD TaO_x grown with a 0.3 sccm O_2 flow rate. The p-Si/TaO_x/Cu-10nm based photocathode produced nearly 52 % CO_2R products at bias of -1.2 V vs RHE while a p-Si/TiO_2

photocathode with the same Cu co-catalyst thickness yielded only H_2 (**Figure 4 (a))** despite its earlier photocurrent onset and higher photocurrent density (**Figure S9**).

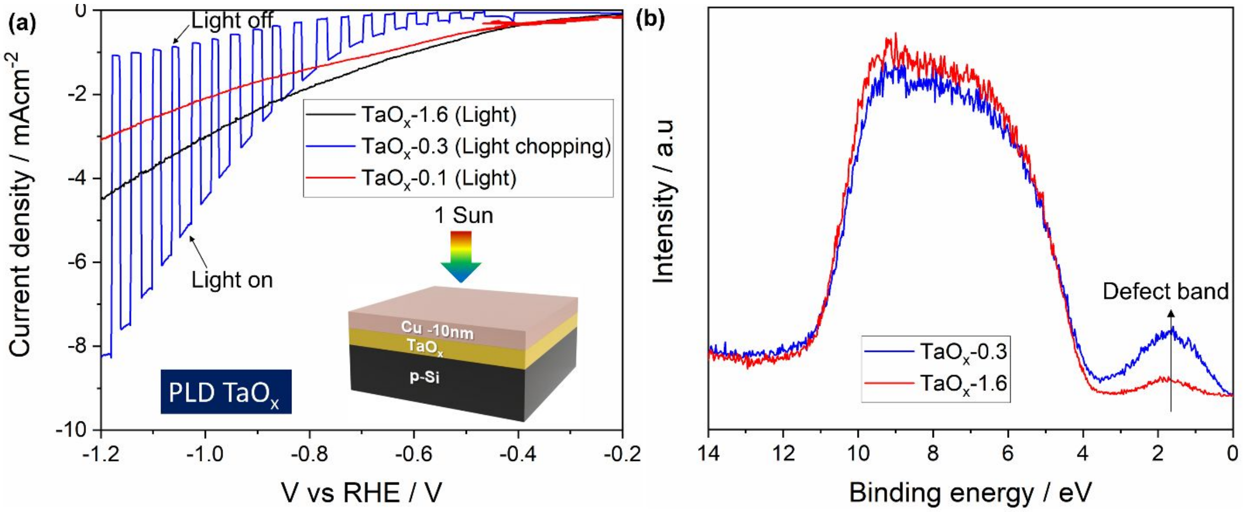

Figure 3. (a) Current density vs Voltage plots for p-Si/TaO$_x$/Cu 10nm photocathodes with TaO$_x$ grown ETLs at different oxygen flow rates under 1 sun illumination in a 0.1 M $KHCO_3$ electrolyte. (b) Valence band spectra of TaO$_x$-0.3 and TaO$_x$-1.6 thin films.

To evaluate the compatibility of TaO$_x$ with other CO_2R catalysts, an Au catalyst was employed to evaluate the CO_2R product distribution. A Ta underlayer was used for the Au catalyst to improve its adhesion to TaO$_x$. The photocurrent density obtained was similar to that of p-Si/TaO$_x$/Cu (**Figure S10**) and the CO_2R products obtained were primarily C1products (CO, $HCOO^-$) as expected for an Au catalyst (**Figure 4 (b)**). Based on these results, TaO$_x$ could be employed as an ETL for p-Si interfaced with both Cu and Au co-catalysts for CO_2R.

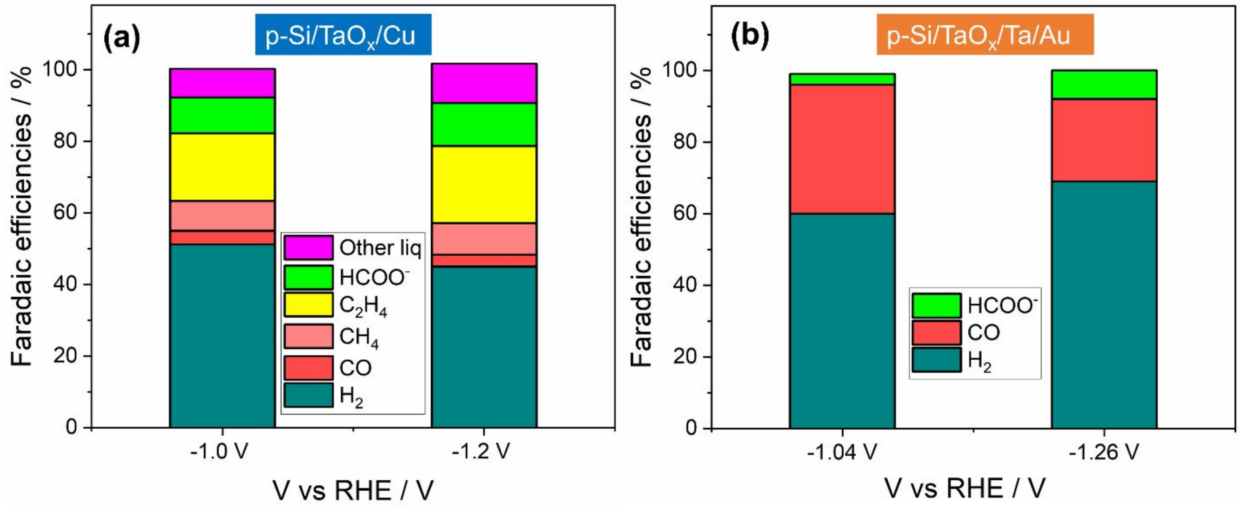

Figure 4. Faradaic efficiencies for (a) p-Si/TaO$_x$/Cu (other liq denotes ethanol and acetate) (b) p-Si/TaO$_x$/Ta/Au photocathodes under 1 sun illumination in 0.1 M KHCO$_3$

Reactive radio frequency (RF) sputtered TaO$_x$ as an ETL for CO$_2$R Si photocathode. Photocathodes were made with TaO$_x$ deposited by reactive RF sputtering, which is a more scalable technique than PLD (**experimental details in supporting information**). A Ta metal target was used and the Ar:O$_2$ ratio in the chamber was used to oxygen substoichiometry of TaO$_x$. **Figure 5 (a)** shows the Ta 4f spectra for the TaO$_x$ films prepared with 2 different Ar:O$_2$ ratios. Similar to the PLD prepared TaO$_x$ films (compare **Figure 2 (b)**), the doublet peaks for Ta^{5+} oxidation state are dominant. However, the film made with a lower O$_2$ partial pressure (99:1 Ar:O$_2$) exhibits a significant peak corresponding to Ta metal suggesting that not all the Ta metal has been oxidized to the +5 oxidation state.

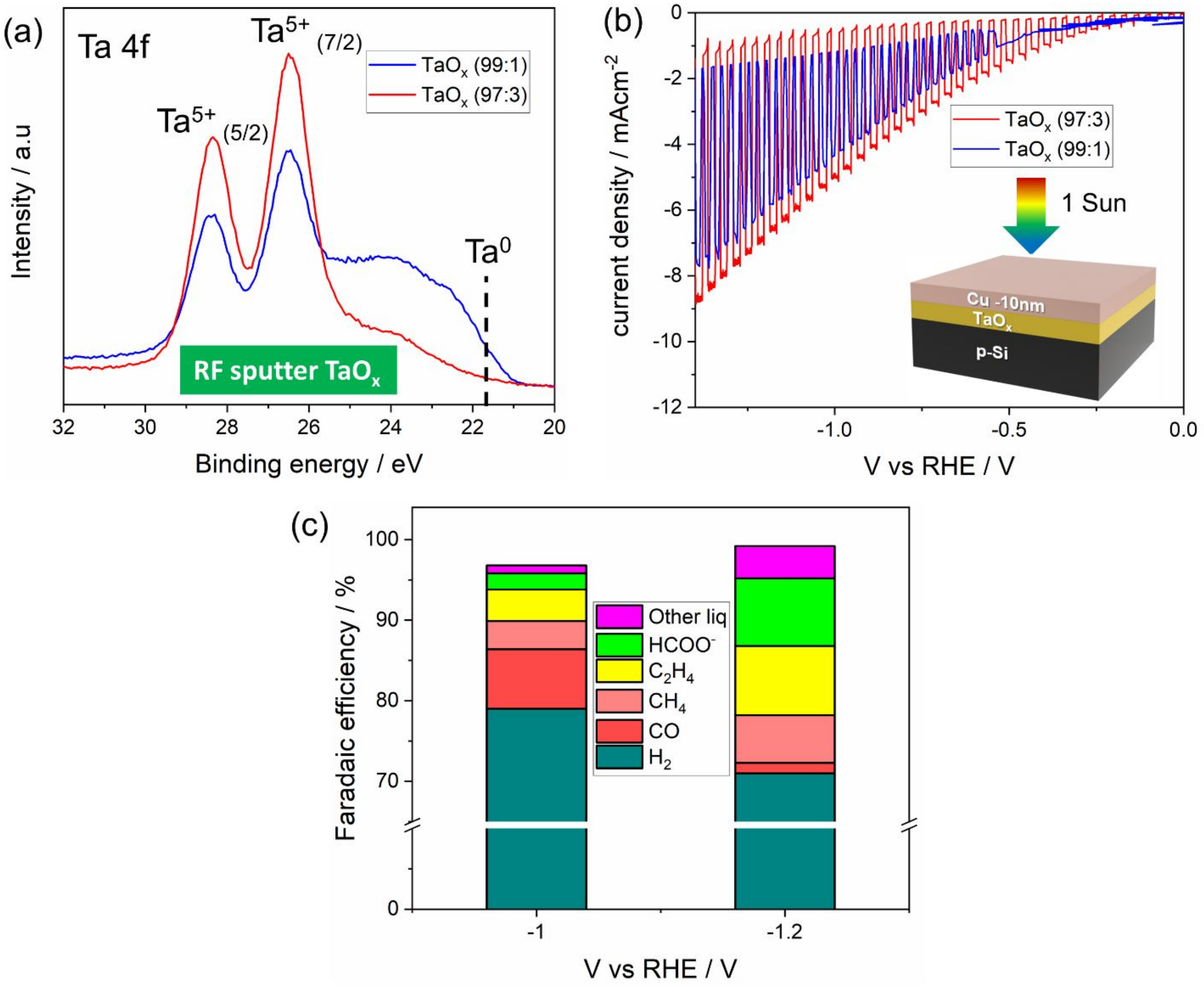

Figure 5. (a) Ta 4f core level spectra of TaO$_x$ prepared by RF sputtering under 2 different Ar: O$_2$ ratio (b) Current density (*J*) vs Voltage (*V*) plots for Si/TaO$_x$(20 nm)/Cu 10 nm under 1 sun illumination in 0.1 M KHCO$_3$ under 2 different Ar:O$_2$ concentration (c) Faradaic efficiencies of CO$_2$R products for Si/TaO$_x$ (20 nm)/Cu10 nm under -1 V and -1.2 V vs RHE (other liq denotes ethanol and acetate).

Next the photoelectrochemical performance of the p-Si/TaO$_x$ (RFsputtered)/Cu photocathodes were evaluated under the same CO$_2$R conditions as p-Si/TaO$_x$ (PLD grown)/Cu photocathodes. Photocathodes fabricated using RF sputtered TaOx had a very smooth surface after deposition of the Cu catalyst (**Figure S11**) and their XRD patterns only exhibited peaks corresponding to Si (**Figure S12**). The photocathode with higher oxygen content (TaO$_x$ 97:3) yielded a marginal higher photocurrent and lower dark current as there is no Ta metal in the film when compared to TaO_x (99:1) (**Figure 5 (b)**). Variation of the TaO_x thickness showed that photocathodes with 20 nm TaO_x yielded better fill factors and photocurrent density despite exhibiting similar substoichiometry **(Figure S13 and S14**). If the TaO_x thickness is too thick as in the case of 40nm then the photocurrent density is lowered probably due to increased series resistance and if the thickness is below 20 nm then the coverage of TaO_x on Si is not uniform. Hence a thickness of 20 nm of TaO_x with 97:3 Ar to O_2 condition was found to be optimum. Upon comparing the champion device of sputtering (TaO_x (97:3)) with PLD champion device (TaO_x-0.3), the sputtering champion device exhibited an earlier photocurrent onset but a marginally lower photocurrent density (**Figure S15**). This could be attributed to an increase in the substoichiometry of TaO_x films prepared by sputtering (**Figure S16**).

Si photocathode with dual ETL: A dual ETL approach has shown promise in water splitting where one ETL serves as a n-type junction layer and the other performs the role of protection and catalyst support.[38] Since TiO_2 has a better band alignment with p-Si, we used it as the primary ETL and sputtered TaO_x on it to take advantage of its higher CO_2R product yield and stability. The photocurrent onset and the photocurrent density of such a dual ETL photocathode is lower in comparison to Si-TiO_2/Cu layer **(Figure 6 (a))**. But the dual ETL photocathode produced more CO_2R products than a Si-TiO_2-Cu as the TiO_2 is buried under $TaO_{x.}$ Since the TiO_2 layer is not fully exposed to the electrolyte under CO_2R conditions, HER activity is suppressed and the catalytic activity could be dominated by the TaO_x/Cu layer **(Figure 6b)**. The dual ETL device was able to combine the earlier photocurrent onset of p-Si/TiO_2/Cu device with the higher CO_2R product selectivity of p-Si/TaO_x/Cu device. The partial current densities towards CO_2R products (CO, CH_4, C_2H_4 and $HCOO^-$) for dual ETL photocathode were only marginally lower than the p-Si-TaO_x-Cu photocathode at -1.0 V vs RHE (**Figure S17**). Having a dual ETL approach would enable photocathode designs where the photovoltage could be improved by employing n-type layer which has a good band alignment with the underlying p-type absorber and simultaneously taking advantage of TaO_x/Cu's stability and higher yield of CO_2R products.

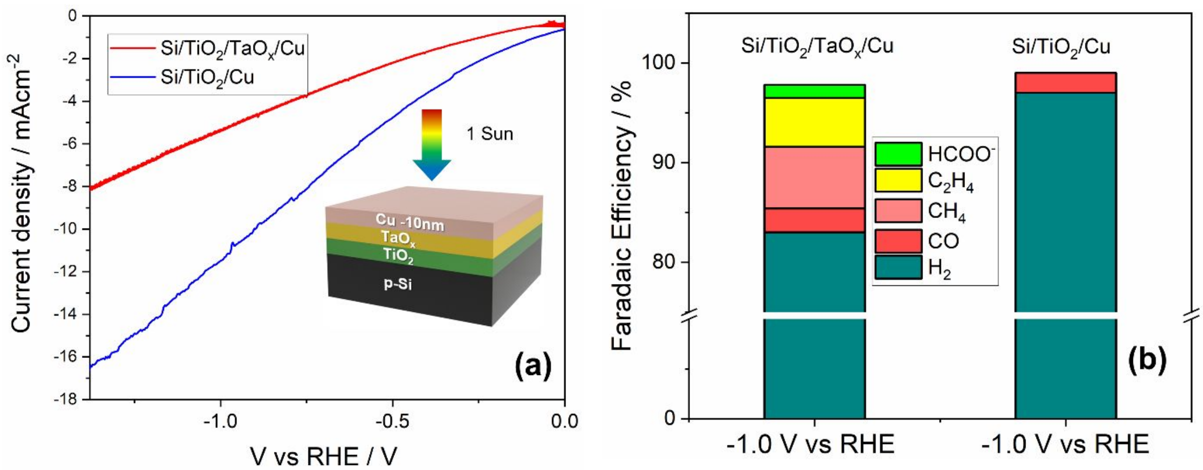

Figure 6. (a) Current density (*J*) vs Voltage (*V*) plots for Si/TiO_2/Cu and Si/TiO_2/TaO_x (97:3)/Cu under 1 sun illumination in 0.1 M $KHCO_3$ (b) Faradaic efficiencies of CO_2R products for Si/TiO_2/Cu and Si/TiO_2/TaO_x(97:3)/Cu The thickness of Cu catalyst used was 10 nm for both photocathodes.

Photovoltage: Finally, we fabricated a n^+Si/TaO_x (97:3)/Cu dark cathode (black curve in Figure 7) so that we can compare the onset of the dark catalytic current to photocurrent onset of a p-Si/TaO_x/Cu photocathode (Figure 7 (a)). There are no reports in literature to the best of our knowledge where p-Si is directly interfaced with TaO_x to form the p-n junction which gives a photovoltage. Instead, most reports in the photovoltaic literature employ n-Si with TaO_x as a surface passivation/electron selective contact.[22] In this work a photovoltage of ~ 300 mV was obtained for p-Si/TaO_x junctions with a Cu CO_2R catalyst (**Figure 7 (a) and Figure S18 (a)**). To improve the photovoltage of these photocathodes, an n^+ implant of p-Si wafers was performed to yield a better-quality junction with RF sputtered TaO_x onto the p-Si/n^+ with a Cu catalyst. This photocathode yielded a higher photovoltage of 430 mV (**Figure 7 (b) and Figure S18 (b)**). Both photovoltage and photocurrent density was increased when a silicon photocathode (n-Si with n^+ and p^+ implanted contacts[20]) were employed with a RF-sputtered TaO_x ETL and Cu catalyst (**Figure 7 (c) and Figure S18 (c)**) showing the broad applicability of RF-sputtered TaO_x as an ETL for photocathodes.

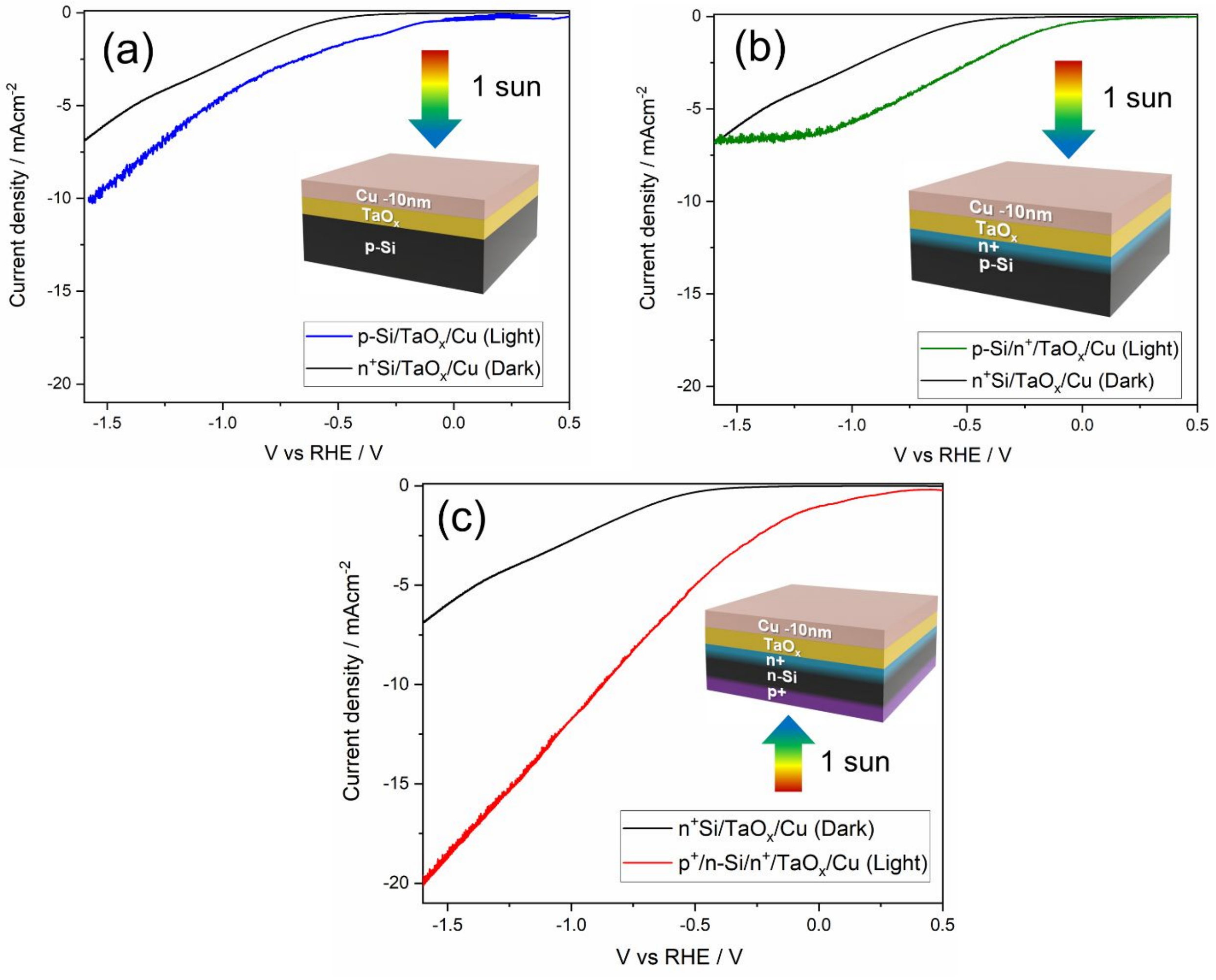

Figure 7. Current density vs voltage plots for (a) $n^+Si/TaO_x/Cu$ (dark cathode) and $p\text{-}Si/TaO_x/Cu$ (photocurrent), (b) $n^+Si/TaO_x/Cu$ (dark cathode) and $p\text{-}Si/n^+/TaO_x/Cu$ (photocathode) and (c) $n^+Si/TaO_x/Cu$ (dark cathode) and $p^+/n\text{-}Si/n^+/TaO_x/Cu$ (photocathode).

Long-term stability of p-Si/TaO$_x$/Cu photocathodes: The long-term stability of p-Si/TaO$_x$/Cu photocathodes over a period of 300 mins was evaluated by the time evolution of CO$_2$R gaseous products (**Figure S19**). Samples with RF sputtered TaO$_x$ were chosen as it is more scalable synthesis technique than PLD and has a higher potential for commercialization. The surface of the photocathode became more rougher after the long term CO$_2$R electrolysis (**Figure S20**). A fairly stable evolution of CO$_2$R products was observed for at least for a period of 120 mins after which the faradaic efficiencies for the CO$_2$R products decreased. The electrolyte was changed after 225 mins when no ethylene production was observed. Although there was a decrease in the Cu signal from XPS after operation (**Figure S21**), the lack of ethylene production could not be just attributed to loss of Cu catalyst. After CO$_2$R photoelectrolysis, contact angle measurements were performed to investigate the hydrophobicity of the photocathode and it was observed that the surface of the photocathode (TaO$_x$/Cu) became more hydrophilic after CO$_2$R (**Figure S22)**). In the CO$_2$R electrolysis literature, the change in hydrophobicity has been attributed to minor CO$_2$R product polymerization (acrolein to polyacrylic acid) on the surface of the Cu catalyst.[39] It is conceivable that this effect is occurring here, as well. In stability tests, we used a Pt counter electrode but found that Pt migration to the PEC surface strongly affected the results which are mitigated by using a graphite counter electrode (see discussion in SI).

Using a graphite counter electrode resulted in continued ethylene production even after 300 mins of operations (and good photocurrent stability **Figure S23**) when compared to Pt counter electrode which required change of electrolyte after 225 mins in order to sustain ethylene production (**Figure 8 (a)**). Further no Pt 4f peak (71 eV) was observed on the photocathode surface after 5 hours of operation when employing a graphite counter electrode (**Figure S24**). The surface of p-Si/TaOx/Cu after operation were still hydrophilic (same as the case with Pt counter electrode) hinting that the long-term stability of the photocathode was not significantly affected by the change in hydrophobicity of the surface but rather the crossover of Pt from the counter electrode was the main reason for decreased C_2H_4 production (**Figure 8 (b) and (c)**).

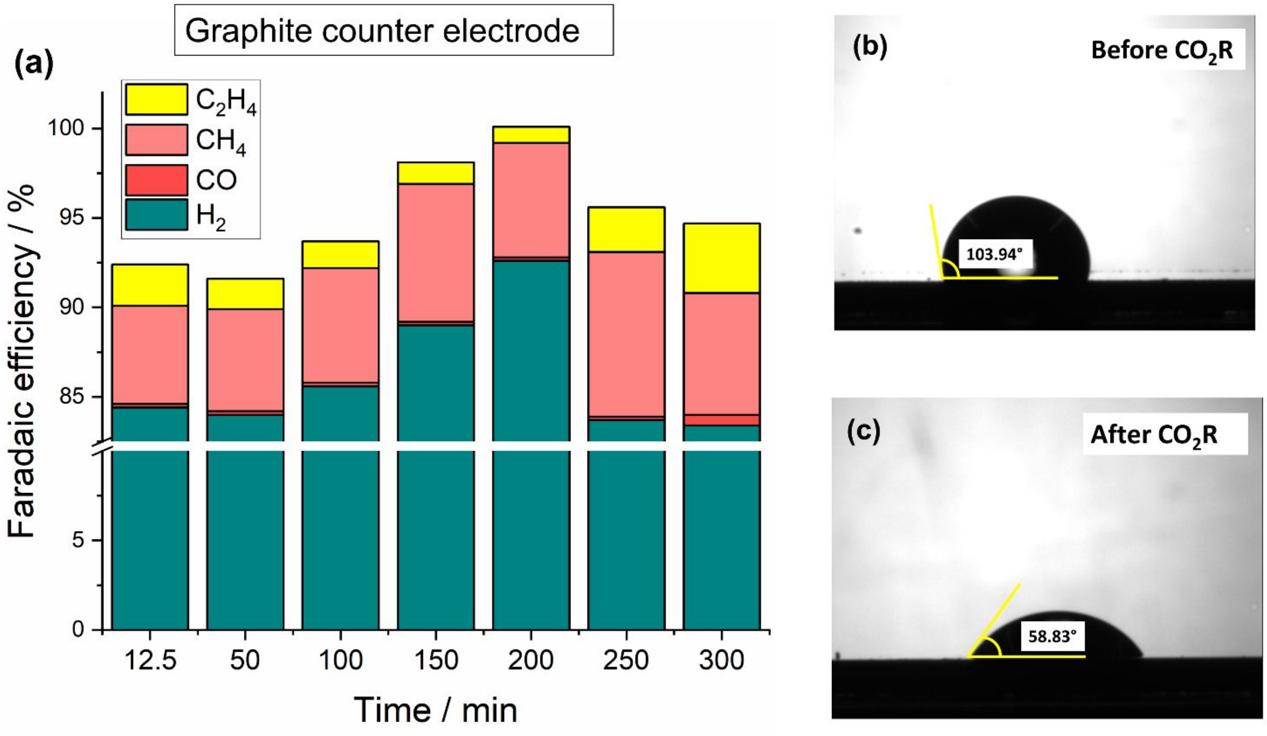

Figure 8. (a) Gaseous CO_2R product distribution as a function of time for Si/TaO_x(97:3)/Cu10nm photocathode under 1 sun illumination in 0.1M $KHCO_3$ at -1.2 V vs RHE with a graphite counter electrode where the production of C_2H_4 remained steady after 300 mins of operation without any need of electrolyte change. Contact angle measurements of p-Si/TaO_x/Cu photocathode with a Pt counter electrode during CO_2R measurements for (b) before CO_2R and (c) after CO_2R operation for 300 mins.

Techno-economic analysis of Si-TaO_x-Cu photocathode: The selectivity of Si-TaO_x-Cu photocathode towards carbon-containing products incentivized to conceptually design a large-scale photocatalytic system that could be used for production of carbon-rich gas streams from abundant, biogenic CO_2 (**Figure. 9(a)**). One of the anticipated bottlenecks towards the deployment of CO_2-

based systems is the low concentration of CO_2 in the ambient air.[40] The availability of CO_2 in oceans is significantly higher.[41] We thus conceptualized a system where ocean water, source of preconcentrated CO_2, circulates through photoelectrochemical systems, and CO_2 is converted into a stream of ethylene, carbon monoxide, methane, and hydrogen, being a useful input to various chemical manufacturing processes.[42] Such a system would require a minimum input of renewable electricity sourced from solar panels or windmills, as a significant amount of energy is being supplied via direct sunlight irradiation.

Looking towards this large-scale scenario, we sought to understand whether proposed catalyst deposition method could be effectively scaled up, and we assessed the cost of production of a system incorporating a thin TaO_x-Cu layer deposited on silicon wafer, using pilot plant scale/ semi-industrial coefficients for energy and gases use during physical vapor deposition process[43,44], and most recent price indicators for each component of the electrocatalytic system.[45–48] While other deposition methods reported here, such as RF sputtering, could further reduce the catalyst production cost, selecting physical vapor deposition (PVD) as reference allows to assess a less favorable scenario thus reduce the risk of overestimating the potential of the photocathode, being current at an early development stage. Given the excellent reduction of the thickness of the catalyst, the manufacturing cost becomes practically reduced to the cost of the silicon wafer and the membrane (**Figure 9(b)**), contributing together to >95% of the cost of the photoelectrode system (detail cost contributions in SI). Intriguingly, similar results have been obtained for Au-based electrodes (SI), showing that thin catalyst layers allow to drastically minimize the cost of metals used in catalyst development.

Looking at the return on investment into the proposed photoelectrochemical system, we deployed a recent protocol for the assessment of emerging electrolysis technologies (method details in SI) [49]. Our assessment is based on a model of a Si-TaO_x-Cu electrolyzer where 75% of supplied

CO_2 is being converted to a carbon-rich product, under experimentally reported 0.01 A cm^{-2} of current density and applying an external voltage of 1.2 V. We assumed an average market price for this ethylene-rich stream, current renewable electricity price[42] between 0.02 – 0.05 $/kWh, and a broad range of CO_2 credit being paid for the avoided emissions of CO_2 (our system allows to avoid emissions of petroleum-based CO_2 by producing chemicals from biogenic CO_2). The sensitivity analysis **(Figure 9(c))** demonstrates that in presence of CO_2 credit schemes, return on investment is even less than 2 years, what provides an incentive for further research and optimization of CO_2 utilization methods. The decrease of the price of renewable electricity alone would not be sufficient to support these innovative approaches (see the grey area in **Figure 9 (c)**), depicting non-viable scenarios), and the availability of CO_2 credit will be critical for the growth of photoelectrochemical methods. Still, we need as well to address several scale-up challenges: demonstrate the capability to achieve increased CO_2 conversion level and avoid the formation of liquid products which will be more difficult to separate than the gaseous stream that we focus on. Importantly, electrolysis of sea water with a high concentration of salts might also lead to formation of chlorine on the anode. However, the studies focusing on the production of hydrogen from sea water demonstrated that it is possible to effectively block chlorine formation by the addition of MnO_x into the anode structure.[50] Achieving the outstanding techno-economic metrics for the PEC system described here will thus necessitate coordinated efforts in further development of more scalable cathodes, anodes and related chemical process design.

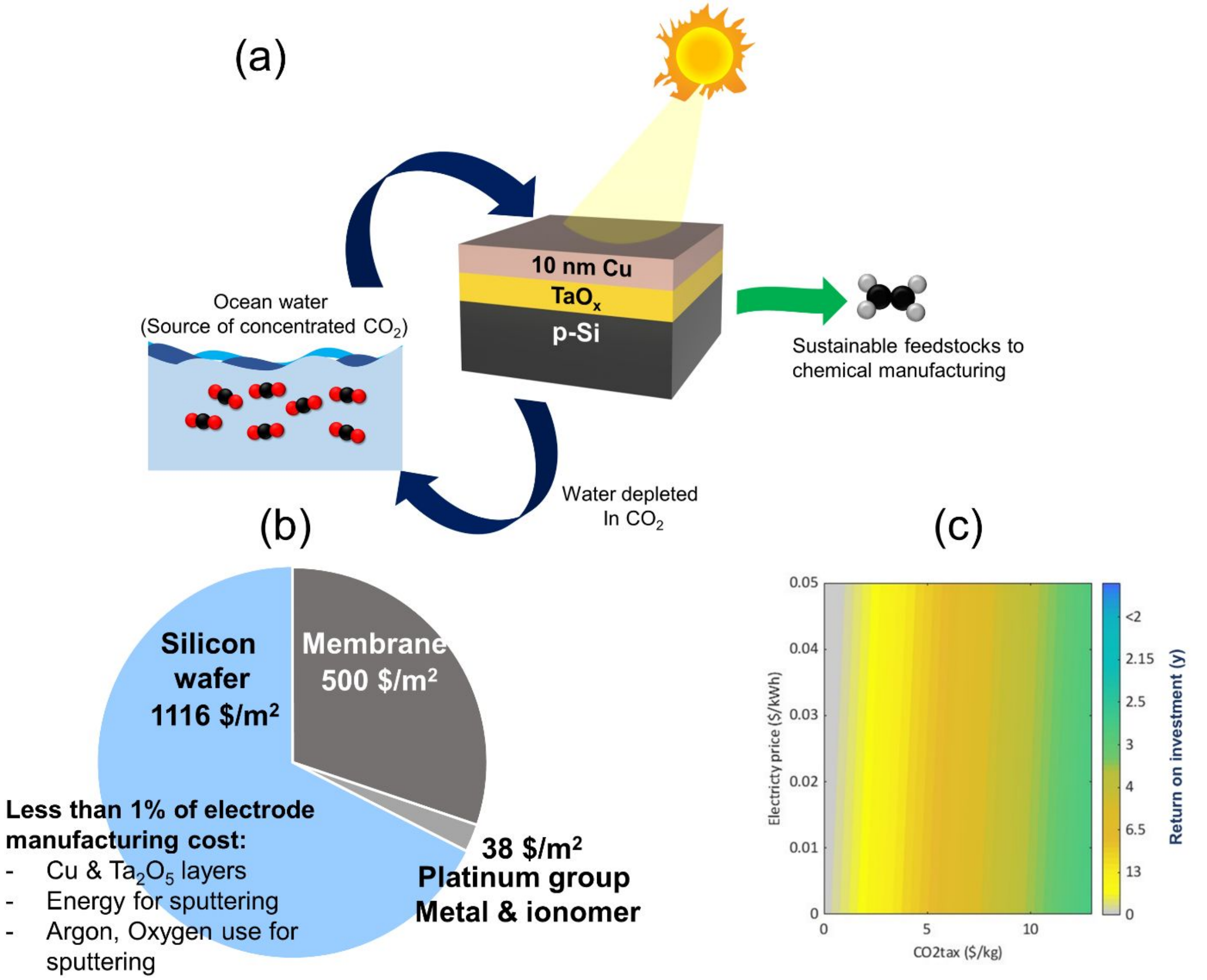

Figure 9. Conceptualized scale-up and techno-economic analysis (TEA) of systems incorporating Si/TaO_x/Cu photocathodes: (a) concept of biogenic CO_2- based manufacturing systems, (b) manufacturing cost for Si/TaO_x/Cu photocathodes based on pilot-plant/semi industrial scale coefficient for energy and gases uses during PVD process, (c) sensitivity analysis for the return on investment for the entire photoelectrochemical system, as a function of renewable electricity price and imposed credit for avoided CO_2 emissions. Grey area depicts scenarios which are not economically viable. Methodology details are given in the SI.

CONCLUSIONS

In summary, TaO_x was used as an ETL for Si photocathodes (Si/TaO_x p-n junction) for the first time for CO_2R. We first identified the major drawback of employing TiO_2 as an ETL (reduction of TiO_2 to Ti metal and evolution of H_2) and then synthesized TaO_x by 2 different synthesis techniques (PLD and RF sputtering). The electron selectivity of the TaO_x ETLs was tuned by controlling the oxygen partial pressures during thin film deposition for both techniques. Si/TaO_x/Cu photocathodes yielded much higher CO_2R products (52% for PLD TaO_x and 30% for RF sputtered TaO_x)) when compared with Si/TiO_2/Cu photocathode. We also demonstrated a dual ETL layer (Si/TiO_2/TaO_x/Cu) photocathode which could be a possible strategy for other photocathodes to suppress HER and yield more CO_2R products. The photovoltage of silicon photocathodes with TaO_x ETL/Cu catalyst was improved by using implanted contacts (n^+ only on p-Si & n^+ and p^+ contacts on n-Si) from 300 mV to 430-460 mV. For long term stability of these photocathodes, the limiting factor was the Pt crossover from the counter electrode to the Si/TaO_x/Cu photocathode. The photocathode was found to be stable (sustained ethylene production) for ~ 300 mins of CO_2R photoelectrolysis when employing a graphite counter electrode to mitigate Pt crossover. By employing scalable synthesis techniques (RF sputtering for ETLs and Cu catalyst) and simple device architecture without any energy intensive fabrication process (high temperature growth/doping of Si) we have demonstrated an excellent scalability of the system. Our techno-economic analysis outlines pathways to making the photoelectrochemical platform a viable method for decarbonized chemical production, and we determined the scale of CO_2 credits mechanisms necessary to support the growth of photocatalytic field. This work also elucidates possible design strategies of other ETLs for CO_2R photocathode- suppression of HER catalysis, good electronic conductivity and Pourbaix stability. Finally, this work raises the question where there are favorable and/or tunable catalyst-metal oxide support interactions in this type of PEC approach and whether they can be tuned by the choice of metal oxide and by the deposition method. A potential method to investigate such effects would be to use ambient pressure X-ray photoelectron spectroscopy (AP-XPS) to examine the influence of the ETL on the Cu oxidation state under *operando* PEC conditions.

Author Contributions

The manuscript was written through contributions of all authors. All authors have given approval to the final version of the manuscript. RL, RRP, and JWA conceived the experiment. RRP, RL and MK performed the synthesis of TaO_x. RRP did the XPS measurements and RL performed the UPS measurements. Photocathodes were fabricated by RRP and RL. Liquid and Gas CO_2R product quantification was performed by RRP and RL. SS helped with long-term testing of photocathodes and graphics in the paper. IDT performed the XRD measurements. END performed the MEEP simulations. MB performed the technoeconomic analysis (TEA) and wrote the TEA part. RRP and JWA wrote the original draft of the paper. All authors were involved in the reviewing and editing of the draft. JWA was involved in the funding acquisition and project administration.

Conflict of interest

The authors declare no competing financial interests.

ACKNOWLEDGMENT

This material is based on work performed by the Liquid Sunlight Alliance, which is supported by the U.S. Department of Energy, Office of Science, Office of Basic Energy Sciences, Fuels from Sunlight Hub under Award Number DE-SC0021266. Technoeconomic analyses performed by MB were supported by the National Research Foundation (NRF), Prime Minister's Office, Singapore, under its Campus for Research Excellence and Technological Enterprise (CREATE) programme through the eCO2EP project NRF2016-ITC001-005 operated by the Cambridge Centre for

Advanced Research and Education in Singapore (CARES) and the Berkeley Educational Alliance for Research in Singapore (BEARS). RRP acknowledges fellowship support from the Swiss National Science Foundation Early Postdoc Mobility Program (191299). MK acknowledges fellowship support from the Brain Korea 21 Program (BK21 FOUR). END acknowledges fellowship support from EPFL and the Heyning-Roelli Schindler Foundation. IDT acknowledges fellowship support from the Erasmus Foundation.

REFERENCES

1 U. Wurfel, A. Cuevas and P. Wurfel, *IEEE J. Photovoltaics*, 2015, **5**, 461–469.
2 M. Taguchi, A. Yano, S. Tohoda, K. Matsuyama, Y. Nakamura, T. Nishiwaki, K. Fujita and E. Maruyama, *IEEE J. Photovoltaics*, 2014, **4**, 96–99.
3 C. Battaglia, A. Cuevas and S. De Wolf, *Energy Environ. Sci.*, 2016, **9**, 1552–1576.
4 R. V. K. Chavali, S. De Wolf and M. A. Alam, *Prog. Photovoltaics Res. Appl.*, 2018.
5 T. G. Allen, J. Bullock, X. Yang, A. Javey and S. De Wolf, *Nat. Energy*, 2019, **4**, 914–928.
6 G. Campet, C. Puprichitkun and Z. W. Sun, *J. Electroanal. Chem. Interfacial Electrochem.*, 1989, **269**, 435–445.
7 S. Hu, N. S. Lewis, J. W. Ager, J. Yang, J. R. McKone and N. C. Strandwitz, *J. Phys. Chem. C*, 2015, **119**, 24201–24228.
8 S. Chen and L.-W. Wang, *Chem. Mater.*, 2012, **24**, 3659–3666.
9 Y. Lin, C. Battaglia, M. Boccard, M. Hettick, Z. Yu, C. Ballif, J. W. Ager and A. Javey, *Nano Lett.*, 2013, **13**, 5615–5618.
10 Y. Lin, R. Kapadia, J. Yang, M. Zheng, K. Chen, M. Hettick, X. Yin, C. Battaglia, I. D. Sharp, J. W. Ager and A. Javey, *J. Phys. Chem. C*, 2015, **119**, 2308–2313.
11 D. Bae, B. Seger, O. Hansen, P. C. K. Vesborg and I. Chorkendorff, *ChemElectroChem*, 2019, **6**, 106–109.
12 Y. Hori, A. Murata and R. Takahashi, *J. Chem. Soc. Faraday Trans. 1 Phys. Chem. Condens. Phases*, 1989, **85**, 2309.
13 Y. Hori, in *Modern Aspects of Electrochemistry*, Springer New York, New York, NY, 2008, vol. 29, pp. 89–189.
14 Y. Chen, C. W. Li and M. W. Kanan, *J. Am. Chem. Soc.*, 2012, **134**, 19969–19972.
15 N. Han, Y. Wang, H. Yang, J. Deng, J. Wu, Y. Li and Y. Li, *Nat. Commun.*, 2018, **9**, 1320.
16 L. Fan, C. Xia, P. Zhu, Y. Lu and H. Wang, *Nat. Commun.*, 2020, **11**, 3633.
17 S. Nitopi, E. Bertheussen, S. B. Scott, X. Liu, A. K. Engstfeld, S. Horch, B. Seger, I. E. L. L. Stephens, K. Chan, C. Hahn, J. K. Nørskov, T. F. Jaramillo and I. Chorkendorff, *Chem.*

Rev., 2019, **119**, 7610–7672.

18 R. Hinogami, Y. Nakamura, S. Yae and Y. Nakato, *J. Phys. Chem. B*, 1998, **102**, 974–980.

19 J. Qiu, G. Zeng, M.-A. Ha, M. Ge, Y. Lin, M. Hettick, B. Hou, A. N. Alexandrova, A. Javey and S. B. Cronin, *Nano Lett.*, 2015, **15**, 6177–6181.

20 Gurudayal, J. W. Beeman, J. Bullock, H. Wang, J. Eichhorn, C. Towle, A. Javey, F. M. Toma, N. Mathews and J. W. Ager, *Energy Environ. Sci.*, 2019, **12**, 1068–1077.

21 P. B. Pati, R. Wang, E. Boutin, S. Diring, S. Jobic, N. Barreau, F. Odobel and M. Robert, *Nat. Commun.*, 2020, **11**, 3499.

22 Y. Wan, S. K. Karuturi, C. Samundsett, J. Bullock, M. Hettick, D. Yan, J. Peng, P. R. Narangari, S. Mokkapati, H. H. Tan, C. Jagadish, A. Javey and A. Cuevas, *ACS Energy Lett.*, 2018, **3**, 125–131.

23 Y. Wan, J. Bullock and A. Cuevas, *Sol. Energy Mater. Sol. Cells*, 2015, **142**, 42–46.

24 M. T. Greiner, M. G. Helander, W.-M. Tang, Z.-B. Wang, J. Qiu and Z.-H. Lu, *Nat. Mater.*, 2012, **11**, 76–81.

25 T. Wang, S. Liu, H. Li, C. Li, Z. Luo and J. Gong, *Ind. Eng. Chem. Res.*, 2019, **58**, 5510–5515.

26 S. Riyajuddin, J. Sultana, S. A. Siddiqui, S. Kumar, D. Badhwar, S. S. Yadav, S. Goyal, A. Venkatesan, S. Chakraverty and K. Ghosh, *Sustain. Energy Fuels*, 2022, **6**, 197–208.

27 A. Jain, S. P. Ong, G. Hautier, W. Chen, W. D. Richards, S. Dacek, S. Cholia, D. Gunter, D. Skinner, G. Ceder and K. A. Persson, *APL Mater.*, 2013, **1**, 11002.

28 A. K. Singh, L. Zhou, A. Shinde, S. K. Suram, J. H. Montoya, D. Winston, J. M. Gregoire and K. A. Persson, *Chem. Mater.*, 2017, **29**, 10159–10167.

29 J.-Y. Zhang and I. W. Boyd, *Appl. Surf. Sci.*, 2000, **168**, 234–238.

30 X. M. Wu, P. K. Wu, T. -M. Lu and E. J. Rymaszewski, *Appl. Phys. Lett.*, 1993, **62**, 3264–3266.

31 S. J. Song, T. Park, K. J. Yoon, J. H. Yoon, D. E. Kwon, W. Noh, C. Lansalot-Matras, S. Gatineau, H.-K. Lee, S. Gautam, D.-Y. Cho, S. W. Lee and C. S. Hwang, *ACS Appl. Mater. Interfaces*, 2017, **9**, 537–547.

32 Y. R. Denny, T. Firmansyah, S. K. Oh, H. J. Kang, D.-S. Yang, S. Heo, J. Chung and J. C. Lee, *Mater. Res. Bull.*, 2016, **82**, 1–6.

33 R. J. Bondi, M. P. Desjarlais, A. P. Thompson, G. L. Brennecka and M. J. Marinella, *J. Appl. Phys.*, 2013, **114**, 203701.

34 S. Boughaba, M. U. Islam, G. I. Sproule and M. J. Graham, *Surf. Coatings Technol.*, 1999, **120–121**, 757–764.

35 E. Atanassova and D. Spassov, *Appl. Surf. Sci.*, 1998, **135**, 71–82.

36 E. Atanassova, T. Dimitrova and J. Koprinarova, *Appl. Surf. Sci.*, 1995, **84**, 193–202.

37 Y. Li, S. Sanna, K. Norrman, D. V. Christensen, C. S. Pedersen, J. M. G. Lastra, M. L. Traulsen, V. Esposito and N. Pryds, *Appl. Surf. Sci.*, 2019, **470**, 1071–1074.

38 A. Paracchino, V. Laporte, K. Sivula, M. Grätzel and E. Thimsen, *Nat Mater*, 2011, **10**, 456–461.

39 M. K. Kovalev, H. Ren, M. Zakir Muhamad, J. W. Ager and A. A. Lapkin, *ACS Energy Lett.*, 2022, **7**, 599–601.

40 O. S. Bushuyev, P. De Luna, C. T. Dinh, L. Tao, G. Saur, J. van de Lagemaat, S. O. Kelley and E. H. Sargent, *Joule*, 2018, **2**, 825–832.

41 Y. Wu, D. C. E. Bakker, E. P. Achterberg, A. N. Silva, D. D. Pickup, X. Li, S. Hartman, D. Stappard, D. Qi and T. Tyrrell, *Commun. Earth Environ. 2022 31*, 2022, **3**, 1–11.

42 M. H. Barecka, J. W. Ager and A. A. Lapkin, *iScience*, 2021, **24**, 102514.

43 K. Kawajiri, K. Tahara and S. Uemiya, *Resour. Environ. Sustain.*, 2022, **7**, 100047.

44 M. Barecka, A. Zieminska and I. Zbicinski, *INREP Proj. Rev. http//www.inrep.eu/files/TCO%202017/INREP_TCO2017_Presentation_TUL_170921.pdf.*

45 Statista, Tantalum price 2021 | Statista, https://www.statista.com/statistics/1009173/tantalum-price/.

46 MacroTrends, Copper Prices - 45 Year Historical Chart | MacroTrends, https://www.macrotrends.net/1476/copper-prices-historical-chart-data.

47 M. Tyson, Silicon Wafer Prices Expected to Increase by up to 25% by 2025 | Tom’s Hardware, https://www.tomshardware.com/news/silicon-wafer-prices-expected-to-rise-by-up-to-25-by-2025.

48 A. Mayyas, M. Ruth, B. Pivovar, G. Bender and K. Wipke, Manufacturing Cost Analysis for Proton Exchange Membrane Water Electrolyzers, https://www.nrel.gov/docs/fy10osti/72740.pdf.

49 M. H. Barecka, J. W. Ager and A. A. Lapkin, *STAR Protoc.*, 2021, **2**, 100889.

50 J. G. Vos, T. A. Wezendonk, A. W. Jeremiasse and M. T. M. Koper, *J. Am. Chem. Soc.*, 2018, **140**, 10270–10281.